

RSC Advances



This is an *Accepted Manuscript*, which has been through the Royal Society of Chemistry peer review process and has been accepted for publication.

Accepted Manuscripts are published online shortly after acceptance, before technical editing, formatting and proof reading. Using this free service, authors can make their results available to the community, in citable form, before we publish the edited article. This *Accepted Manuscript* will be replaced by the edited, formatted and paginated article as soon as this is available.

You can find more information about *Accepted Manuscripts* in the [Information for Authors](#).

Please note that technical editing may introduce minor changes to the text and/or graphics, which may alter content. The journal's standard [Terms & Conditions](#) and the [Ethical guidelines](#) still apply. In no event shall the Royal Society of Chemistry be held responsible for any errors or omissions in this *Accepted Manuscript* or any consequences arising from the use of any information it contains.

ARTICLE

Hydrogen-bonded effects on supramolecular blue phase liquid crystal dimeric complexes

Cite this: DOI: 10.1039/x0xx00000x

Chong-Lun Wei,[†] Te-Cheng Chen,[†] Putikam Raghunath,[‡] Ming-Chang Lin[‡] and Hong-Cheu Lin^{*†}Received 00th February 2015,
Accepted 00th March 2015

DOI: 10.1039/x0xx00000x

www.rsc.org/

[†]Department of Materials Science and Engineering, National Chiao Tung University, Hsinchu, Taiwan (ROC)[‡]Center for Interdisciplinary Molecular Science, Department of Applied Chemistry, National Chiao Tung University, Hsinchu, Taiwan (ROC)

In this study, a series of novel asymmetric hydrogen-bonded (H-bonded) dimeric complexes **D/P** and **D/P*** (proton donors **D** = **A**, **A***, **AF** and **AF***) were synthesized and self-assembled by appropriate molar ratios of H-donors (**A**, **A***, **AF** and **AF***) and H-acceptors (**P** and **P***). In addition, the influences of the lateral fluoro-substituent of H-donors, the number (along with the position) of chiral centers and the molar ratio of H-donors and H-acceptors on the mesophasic behaviours (e.g., BPs) of asymmetric H-bonded dimeric complexes are investigated. Interestingly, the blue phase (i.e., BPI) was observed in complexes **A*/P**, **A*/P***, **AF*/P** and **AF*/P*** containing at least a chiral center in H-donors (**A*** and **AF***), including the widest BPI ranges of complexes **AF*/P*** (ca. 6°C and 13°C for 1:1 and 3:1 mol., respectively). For the first time, the hydrogen-bonded effects on supramolecular blue phase LCs are compared with their analogous covalent diads. Based on our theoretical calculation, we discovered that the bent angle plays an important role to manipulate the existence of the blue phase, which is preferred to appear at the bent angle within 132.1°–152.9°. Hence, owing to inappropriate bent angles, both H-bonded dimeric complex **A/P*** and covalent diad **A*-P** (with bent angles of 162.0° and 126.5°, respectively) did not possess any blue phase.

Introduction

The blue phase (BP) was discovered by Reinitzer and Lehmann in 1888, where an unusual blue light scattering phenomenon was shortly observed upon cooling from the isotropic phase (at the transition to the chiral nematic phase) in cholesteryl benzoate.¹ In these days, blue phase liquid crystals (BPLCs) have aroused attention in liquid crystal (LC) science due to their unique optical and electro-optical behaviors,² such as selective reflections of circularly polarized light without birefringence. As alluded to above, BPLCs have several advantages:³ including fast response time (about sub-millisecond), no alignment layer required,⁴ and no typical birefringence. Therefore, BPLCs are potential materials to be used in liquid crystal displays (LCDs) and fast responsive modulators.^{5–8} However, BPs exhibited at very narrow temperature ranges (usually about 1 K) and appeared at high temperatures,⁹ which were usually observed between the isotropic phase and chiral nematic (**N***) phase upon cooling. As reported, BPLCs were aggregated into internal helical alignments as “double twisted cylinders (DTC)” with three types of packing structures,^{10,11} which are categorized into BPI, BPII, and BPIII as follows: BPI is a body-center cubic structure, BPII is a

simple cubic structure^{12,13} and BPIII is the same symmetry as the isotropic phase with an arbitrary orientation.^{14,15} So far, many strategies have been introduced to enlarge the BP temperature range and shift the BPs toward the room temperature.¹⁶ Kikuchi et al. have reported that they used polymers to stabilize the disclination of cubic lattice in BPs and extend the temperature range of BPs over 60°C.¹⁷ Pivnenko's group developed novel dimeric BP materials with two symmetric liquid crystal mesogens, which have the BP phase temperature range ca. 44°C.¹⁸ In the meanwhile, Yoshizawa group introduced a chiral structure of binaphthyl to induce blue phase with the BP temperature range approximately 30°C.¹⁹ In addition, they synthesized T-shaped BPLCs²⁰ and utilized U-shaped oligomers to stabilize BPs successfully.²¹ Yang's group also used nano-particles to stabilize BPs and decrease the V-T hysteresis of BPLCs.²² Moreover, chiral materials were doped into biaxial nematic LCs to induce PBs and extend their BP temperature ranges.²³ Furthermore, a bent-core oxadiazole-based liquid crystal has been reported to exhibit a blue phase with a wide range (ca. 30°C).²⁴

More recently, H-bonds have aroused much attention in novel materials because of the flexible characteristic of H-bonds,^{25–27} and the idea of supermolecules bearing noncovalent bond segments with

higher flexibility, i.e. hydrogen-bonds (H-bonds), was applied to induce BPs^{28,30,32} or stabilize BPs.^{29,31} In addition, hydrogen-bonded bent- and T-shaped dopants (without BPs) were also utilized to stabilize BPs in LC mixtures.²⁹ Yang's group showed that two complimentary liquid crystal moieties self-assembled by hydrogen bonds to form BPLC complexes with a wide BP range ca. 23°C,³⁰ and they also used chiral hydrogen-bonded assemblies to induce and stabilize BPs successfully.³¹ Besides, Zhang's group used rod-shaped hydrogen-bonded supermolecules to induce BPs.³² However, no comparisons between analogous H-bonded and covalent structures on the mesophasic properties of BPs and the BP range have been developed so far.

In this study, a series of asymmetric H-bonded dimeric complexes were synthesized and self-assembled by different molar ratios of proton donors and acceptors. Interestingly, the blue phase (i.e., BPI) was only induced in supramolecular complexes containing a chiral center in H-donors. For the first time, the hydrogen-bonded effects on supramolecular blue phase LCs are compared with their analogous covalent diads.³³ In addition, the influences of the position of the chiral center (on H-donor and/or H-acceptor) and the lateral fluoro substituent on the BP temperature range were investigated systematically.

Experimental

Chemical analysis

¹H NMR spectra were recorded on a Bruker Unity 300 MHz spectrometer using DMSO-d₆, CDCl₃ and THF-d₈ as solvents. Elemental analyses (EA) were performed on a Heraeus CHN-OS RAPID elemental analyzer.

Molecular simulation method

To gain insight into the electronic structures of eight asymmetric H-bonded dimeric complexes **D/P** and **D/P*** (where **D** = **A**, **A***, **AF** and **AF***) complexes, we have carried out density functional theory (DFT) calculations by using the Gaussian09 software package.³⁴ Geometry optimization of all the ground state hydrogen-bonded structures was done by B97D Grimme's functional including dispersion corrections³⁵ using the standard 6-31G(d,p) basis set. It was found that the performance of B97D method is remarkably good and reaching average on the CCSD(T) accuracy for noncovalently bound systems including many pure van der Waals complexes.³⁵ The obtained minima are further confirmed by vibrational frequency calculations at the same level; only the lowest energy conformation is reported here. The electrostatic surface potential (ESP) was calculated using the Merz–Singh–Kollman (MK) scheme³⁶ at the B97D/6-31G(d,p) level of theory.

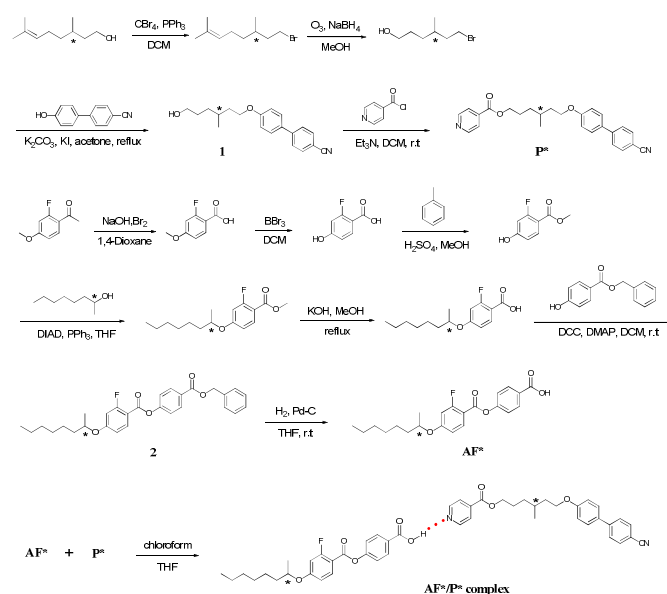
Liquid-crystalline and physical properties

Mesophasic textures of eight final asymmetric H-bonded dimeric complexes were characterized by polarizing optical microscopy (POM) using a Leica DMLP equipped with a temperature control hot stage (Mettler Toledo FP82HT). Temperatures and enthalpies of phase transitions were determined by differential scanning

calorimetry (DSC, model: Perkin Elmer Pyris 7) under N₂ at a heating and cooling rate of 1 °Cmin⁻¹. Infrared (IR) spectra were investigated by Perkin-Elmer Spectrum 100 instrument. Synchrotron powder X-ray diffraction (XRD) measurements were performed at beam-line BL17A equipped with magnetic of the National Synchrotron Radiation Research Center (NSRRC), Taiwan, where the wavelength of X-ray was 1.33336 Å. The powder samples were packed in a capillary tube and heated by a heat gun, for which the temperature controller is programmable by a PC with a PID feedback system. The scattering angle theta was calibrated by a mixture of silver behenate and silicon. Helical twisting power (HTP) measurements of H-bonded dimeric complexes and analogous covalent diads were performed using Cano wedge cells (see Table 3 and Table S2); the commercial LC E7 (Merck) were used as a host.

Preparation of materials

The synthesis of H-bonded dimeric complex **AF*/P*** was shown in Scheme 1.



Scheme 1 Synthesis of asymmetric H-bonded dimeric complexes **AF*/P***.

(S)-4-((2-Fluoro-4-(octan-2-yloxy)benzoyl)oxy)benzoic acid, (AF*). Into a 500 ml round bottom two-neck flask compound **2** (2.0 g, 4.3 mmol) and 10 % Pd / C (0.2 g) catalyst were stirred in THF (200 ml) under hydrogen at room temperature for overnight. The catalyst was removed by filtration through Celite and washed with THF. The solvent was removed by evaporation under reduced pressure and the crude product recrystallized by THF / hexane to give light yellow solid of **AF***, yield 89 %. ¹H NMR (300 MHz, CDCl₃) δ (ppm) : 11.01 (s, 1H, Ar-COOH), 8.06 (d, 2H, Ar-H), 8.02 (t, *J* = 8.4 Hz 1H, Ar-H), 7.32 (m, 2H, Ar-H), 6.97 (dd, *J* = 9.0 Hz 1H, Ar-H), 6.74 (dd, *J* = 9.0 Hz 1H, Ar-H), 6.68 (dd, *J* = 9.0 Hz 1H, Ar-H), 4.43 (m, 1H, -OCH-), 1.70 (m, 1H, -CH₂-), 1.61 (m, 1H, -CH₂-), 1.41-1.26 (m, 11H, -CH₂CH₃), 0.86 (t, *J* = 6.3 Hz 3H, -CH₃). Anal. calcd for C₂₂H₂₅FO₅: C, 68.03, H, 6.49; found: C, 68.33, H, 6.41 %.

(S)-6-((4'-cyano-[1,1'-biphenyl]-4-yl)oxy)-4-methylhexyl isonicotinate, (**P***). A mixture of compound **1** (2g, 6.78 mmol), isonicotinoyl chloride hydrochloride (1.44 g, 8.15 mmol) and triethylamine (2.36 ml) was dissolved in dry dichloromethane (DCM) under nitrogen for 8 h at room temperature. After work up, the solvent was extracted with water / DCM and organic liquid layer was dried over anhydrous magnesium sulphate. After removal of the solvent by evaporation under reduced pressure, the residue was purified by column chromatography and recrystallized from THF/hexane to afford compound **P*** was obtained as a light yellow solid in 63% yield. ¹H NMR (300 MHz, CDCl₃): δ (ppm) 8.77 (d, J=4.2Hz, 2H, Ar-H), 7.91 (m, 6H, Ar-H), 7.69 (d, J=8.8Hz, 2H, Ar-H), 7.02 (d, J=8.9Hz, 2H, Ar-H), 4.41 (t, J=6.3Hz, 2H, -OCH₂), 4.01 (t, J=6.4Hz, 2H, -OCH₂), 1.82-1.21 (m, 7H, -CH₂), 1.13 (d, J=6.3Hz, 3H, -CH₃). Anal. calcd for C₂₆H₂₆N₂O₃: C, 75.34, H, 6.32, N, 6.76; found: C, 75.09, H, 6.44, N, 6.69 %.

Preparation of samples

All asymmetric H-bonded dimeric complexes were constructed by mixing appropriate molar ratios of H-donors (**A**, **A***, **AF** and **AF***) and H-acceptors (**P** and **P***) in solutions of chloroform/THF (~2:1 vol), which were self-assembled into supramolecules by evaporating solvents slowly. All eight compounds of H-bonded in asymmetric heterodimers were formed **D/P** and **D/P*** (where **D** = **A**, **A***, **AF** and **AF***) complexes.

Results and discussion

As shown in Fig. 1, a series of asymmetric H-bonded dimeric complexes **D/N** were synthesized and self-assembled by different molar ratios of proton donors (i.e., H-donors **D** = **A**, **A***, **AF** and **AF***) and proton acceptors (i.e., H-acceptors **N** = **P** and **P***), where **A**, *****, **F** and **P** denote acid, chiral, fluoro and pyridyl moieties, respectively. The hydrogen-bonded effects on supramolecular blue phase LCs of asymmetric H-bonded dimeric complexes **D/P** and **D/P*** are compared with their analogous covalent diads (see reference 33), i.e., H-bonded dimeric complexes **A*/P**, **A/P*** and **A*/P*** vs. covalent diads **A*-P**, **A-P*** and **A*-P***, respectively.³³

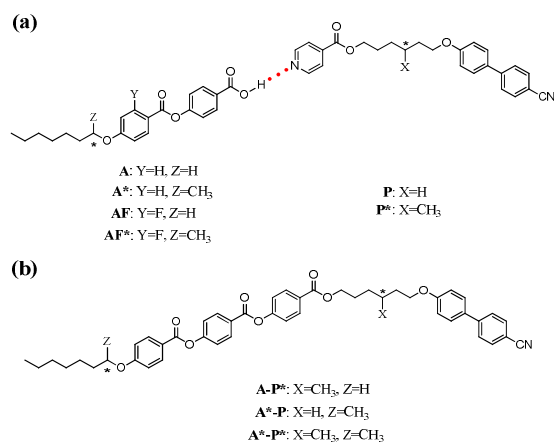


Fig. 1 Molecular structures of (a) asymmetric H-bonded dimeric complexes and (b) their analogous covalent diads (see reference 33).

Chemical synthesis

As illustrated in Fig. 1, H-donors (**A**, **A***, **AF** and **AF***) and H-acceptors (**P** and **P***) of the asymmetric H-bonded dimeric complexes were synthesized according to Schemes S1-S3 (see the supporting information). These compounds with high purities were fully characterized by ¹H-NMR (see the supporting information).

Characterization of H-bonded structures

To study the existence and stability of H-bonds in all asymmetric heterodimers **D/P** and **D/P*** (**D** = **A**, **A***, **AF** and **AF***) complexes can be characterized by FTIR spectroscopy with temperature-various. Taking the asymmetric heterodimers of **AF*/P*** (1:1 mol.) at mole ratio 1:1 of H-donors (**AF***) and H-acceptors (**P***) for example and its constituents **AF*** (H-donor) and **P*** (H-acceptor) are compared in Fig. 2 (a).

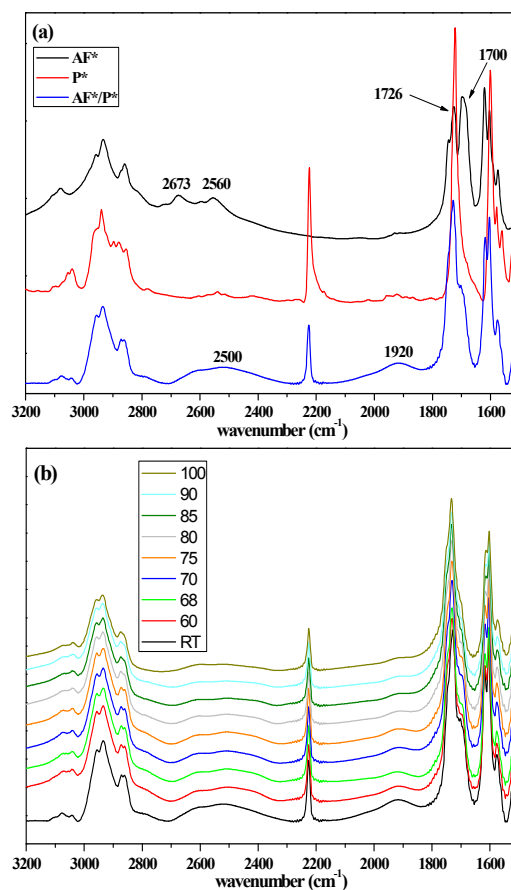


Fig. 2 IR spectra show (a) H-donor **AF***, H-acceptor **P*** and asymmetric H-bonded dimeric complex **AF*/P*** (1:1 mol.). (b) **AF*/P*** (1:1 mol.) complex with variable temperatures (°C).

At room temperature, the O-H bands of pure **AF*** (H-donor) centered at about 2560 cm⁻¹ and 2673 cm⁻¹, when **AF*** (H-donor) and **P*** (H-acceptor) formed H-bonds these characteristic O-H bands disappear and two new broad O-H bands centered at 1920 cm⁻¹ and 2500 cm⁻¹ were observed which indicated that strong H-bonding

formed between the pyridyl and the carboxylic acid groups in the asymmetric heterodimers.^{37,38} On the other hand, carboxylic acid groups C=O stretching vibration appeared at 1700 cm⁻¹ and ester carbonyl groups C=O stretching vibration appeared at 1726 cm⁻¹. In the asymmetric heterodimers of **AF*/P*** (1:1 mol.), a shoulder can be observed in the main peak located at 1726 cm⁻¹. This shoulder is the carbonyl group which is in a less associated state than the pure **AF*** (H-donor) with a weaker carboxylic acid groups C=O stretching vibration appeared at 1700 cm⁻¹.³⁹⁻⁴¹ This is attributed to a carboxylic acid groups C=O stretching vibration at 1700 cm⁻¹ in pure H-donor **AF*** which shifts toward higher wavenumber and overlaps with the band of the ester carbonyl groups at 1726 cm⁻¹ in the asymmetric heterodimers of **AF*/P*** (1:1 mol.). As cooling from the isotropic state to the blue phase I at 68°C, two broad O-H bands centered at 1920 cm⁻¹ and 2500 cm⁻¹ still persist (see Fig. 2) due to the stable H-bonds. These consequences show that hydrogen bonds were formed between **AF*** (H-donor) and **P*** (H-acceptor) as well as other H-bonds asymmetric heterodimers.

Mesophasic and thermal properties

As shown in Tables 1 and 2, the phase transition temperatures, enthalpies and mesophasic ranges of all asymmetric H-bonded dimeric complexes were characterized by polarizer optical microscope (POM) and differential scanning calorimetry (DSC). The transition temperatures of BPs-chiral nematic (N*) were determined by POM (at a cooling rate of 0.5 °Cmin⁻¹) due to their undetectable enthalpy changes by DSC. As the H-bonded complexes were self-assembled by two complimentary components of H-donors (**A**, **A***, **AF** and **AF***) and H-acceptors (**P** and **P***), which formed –OH...N with a stronger tendency in contrast to –OH...C=O– of self-dimeric H-donors.⁴²⁻⁴⁴ However, while H-donors (**A**, **A***, **AF** and **AF***) were added over the stoichiometric amount (50% mol.) of two complimentary components (i.e., up to 66.7, 75 and 80 mole%), the over-supplied H-donors (>50% mol.) will generate self-dimers via the H-bonds of –OH...C=O– after the production of supramolecular complexes. In order to comprehend the configurational influence of various asymmetric H-bonded dimeric complexes, including different numbers (or positions) of chiral centers and lateral fluoro substituent at the aromatic ring, on mesophasic and thermal properties of these eight asymmetric H-bonded dimeric complexes **D/P** and **D/P*** (where **D** = **A**, **A***, **AF** and **AF***) complexes are discussed as follows:

(i) Complexes **D/P** and **D/P*** (where **D** = **A** and **AF** without a chiral center)

The phase transition properties of asymmetric H-bonded dimeric complexes **D/P** and **D/P*** (molar ratio = 1:1; **D** = **A** and **AF**) are demonstrated in Table 1. Without any chiral center on both H-donors and H-acceptors, H-bonded dimeric complexes **A/P** (1:1 mol.) and **AF/P** (1:1 mol.) showed a phase sequence of Iso-nematic (N)-smectic A (SmA)-Crystal. While H-acceptor **P*** was inserted a chiral center to the central linker which connected two different mesogenic units, complexes **A/P*** (1:1 mol.) and **AF/P*** (1:1 mol.) revealed a phase sequence of Iso-chiral nematic (N*)-SmA-Crystal, which induced lower transition temperatures than **A/P** and **AF/P**,

Table 1 Phase transition temperatures (°C)^{a,b} and enthalpies (J/g) of asymmetric H-bonded dimeric complexes containing **A** and **AF**

Complex	Molar ratio (H-donor vs. H-acceptor)	Phase transition temperatures (°C) [Enthalpies (J/g)]		
		Iso	N	SmA
A/P	1:1	186.9 [4.91]	154.9 [3.26]	84.8 [3.01]
AF/P	1:1	168.7 [2.39]	120.3 [4.77]	74.9 [3.61]
A/P*	1:1	177.6 [3.78]	123.8 [4.16]	70.1 [3.21]
AF/P*	1:1	157.5 [4.46]	82.1 [3.62]	60.8 [3.14]

^a Peak temperatures in the DSC profiles obtained during the first heating and cooling cycles at a rate of 1 °Cmin⁻¹. ^b Iso = isotropic phase; BPI = blue phase I; N = nematic phase; N* = chiral nematic phase; SmA = smectic A phase; Cr = crystal. Phase transition temperatures and enthalpies of complexes upon heating and those of pure components **A**, **AF**, **P**, and **P*** are shown in Tables S4 and S5, respectively.

respectively. Due to the larger lateral fluoro substituent than hydrogen,⁴⁵ complexes **AF/P** (1:1 mol.) and **AF/P*** (1:1 mol.) with a lateral fluoro substituent illustrated that lower transition temperatures than **A/P** (1:1 mol.) and **A/P*** (1:1 mol.), respectively. The larger size occupation of both chiral center and lateral fluoro substituent would cause smaller π - π interactions of mesogens and thus to reduce the SmA phase range, i.e., so as to enlarge the N (or N*) phase range. Interestingly, comparing with the other similar chiral complexes of this study no blue phases were observed in both complexes **D/P*** (**D** = **A** and **AF**) due to their smaller biaxial ratios and larger bent angles, which will be explained by molecular modelling later.

(ii) Complexes **D/P** and **D/P*** (where **D** = **A*** and **AF*** with a chiral center)

The phase transition properties of asymmetric H-bonded dimeric complexes **D/P** and **D/P*** (molar ratio = 1:1, 2:1, 3:1 and 4:1; **D** = **A*** and **AF***) are demonstrated in Table 2. **A*/P**, **AF*/P** and **A*/P*** exhibited the phase transition sequence of Iso-blue phase I (BPI)-N*-SmA-Crystal rather than Iso-BPI-N*-Crystal in **AF*/P***, where the SmA phase was totally vanished in **AF*/P*** because of its largest size occupation of two chiral centers and one lateral fluoro substituent to eliminate the smectic layer structure. Surprisingly, all complexes **D/P** and **D/P*** (molar ratio = 1:1, **D** = **A*** and **AF*** with a chiral center) revealed the blue phase (BPI), which is totally different from the previous complexes without a chiral center in H-donors. As shown in Table 2, while H-donors (**A*** and **AF***) were added over the stoichiometric amount (50% mol.) of two complimentary components (i.e., up to 66.7 and 75 mole%), in which the excessive acids (**A*** and **AF***) formed H-bonded dimers, the temperature range of BPI was extended at first. However, as H-donors (**A*** and **AF***) were increased to 80 mole%, the BP temperature range was reduced or even disappeared in complexes **A*/P** (4:1 mol.) and **A*/P*** (4:1 mol.), which might be attributed to the over-supply of **A*** without biaxiality and thus to eliminate the BP and induce the chiral nematic phase (N*) of pure **A*** only. Generally, the widest temperature ranges of BPI were observed at the molar ratio of 3:1 (75 mol%) in all **D/P** and **D/P*** (**D** = **A*** and **AF*** with a chiral center), where the equal molar ratio (1:1 mol.) of acid dimer **D** and supramolecular complexes **D/P** (or **D/P***) were mixed. It is well known that the concentration of chiral dopant was increased and the BP temperature range would be extended.⁴⁶ In fact, the over-

supplied H-donors (>50% mol.) will generate self-dimers and the excessive acid dimers acted as chiral dopants and supplied extra helical twisting power to broaden the BPI temperature range. Oppositely, with over-supplied H-acceptors (**P** and **P***>50% mol.) the excessive H-acceptors (no mesophases shown in Table S5) will not only damage the BP temperature range but also eliminate the occurrence of mesophases (including BP), which have been confirmed by **AF*/P*** with 1:2 and 2:3 molar ratios. Among all complexes in Table 2, **AF*/P*** with 1:1 and 3:1 molar ratios have the broadest BPI temperature ranges of 6.0°C and 13.2°C, respectively, where the lateral fluoro substituent (with a stronger dipole moment) and double chiral centers eliminate the smectic layer structure owing to its larger steric hindrance. On the contrary, complexes **A*/P** (with various molar ratios) have the narrowest corresponding BPI temperature ranges. In addition, with various molar ratios, complexes **AF*/P** have larger BPI temperature ranges than **A*/P***, which suggests that the lateral fluoro substitution (in H-donor) is more favourable to broaden the BPI range than double chiral centers in both H-donor and H-acceptor.

The hydrogen-bonded effects on supramolecular blue phase LCs are compared with their analogous covalent diads, i.e., H-bonded dimeric complexes **A*/P**, **A/P*** and **A*/P*** vs. covalent diads **A*-P**, **A-P*** and **A*-P***, respectively. As illustrated in Table 2, the analogous covalent diad **A*-P*** with double chiral centers has a broader BPI temperature range than H-bonded dimeric complex

Table 2. Phase transition temperatures (°C)^{a,b} and enthalpies (J/g) of asymmetric H-bonded dimeric complexes containing **A*** and **AF*** along with their analogous covalent diads³³

Complex	Molar ratio (H-donor vs. H-acceptor)	Phase transition temperatures (°C) [Enthalpies (J/g)]	ΔT_{BP} (°C)
A*/P	1:1	Iso 150.3 [0.33] BPI 147.9 ^c N* 126.3 [3.61] SmA 64.9 [1.32] Cr 2.4	
	2:1	Iso 133.1 [0.61] BPI 130.1 ^c N* 73.5 [4.25] SmA 52.1 [1.03] Cr 3.0	
	3:1	Iso 106.8 [0.99] BPI 99.3 ^c N* 93.9 [4.92] SmA 46.2 [2.11] Cr 7.5	
	4:1	Iso 150.1 [4.46] N* 80.5 [3.21] Cr 0	
A*/P*	1:1	Iso 89.6 [0.41] BPI 84.9 ^c N* 68.5 [3.41] SmA 41.5 [3.01] Cr 4.7	
	2:1	Iso 123.0 [0.43] BPI 116.1 ^c N* 98.7 [2.88] SmA 44.7 [3.45] Cr 6.9	
	3:1	Iso 132.3 [0.63] BPI 124.1 ^c N* 120.2 [5.69] SmA 72.6 [2.31] Cr 8.2	
	4:1	Iso 140.8 [3.23] N* 80.6 [1.23] Cr 0	
AF*/P	1:1	Iso 96.9 [0.55] BPI 91.3 ^c N* 73.5 [0.31] SmA 35.2 [0.98] Cr 5.6	
	2:1	Iso 106.7 [0.61] BPI 99.6 ^c N* 95.1 [0.35] SmA 50.1 [0.54] Cr 7.1	
	3:1	Iso 120.9 [0.79] BPI 110.9 ^c N* 92.4 [0.52] SmA 70.3 [0.72] Cr 10.0	
	4:1	Iso 126.1 [0.82] BPI 120.8 ^c N* 72.6 [0.56] Cr 5.3	
AF*/P*	1:1	Iso 70.3 [0.52] BPI 64.3 ^c N* 42.3 [1.42] Cr 6.0	
	2:1	Iso 103.5 [0.62] BPI 95.0 ^c N* 62.4 [0.95] Cr 8.5	
	3:1	Iso 109.2 [0.56] BPI 96.0 ^c N* 61.8 [1.02] Cr 13.2	
	4:1	Iso 113.7 [0.58] BPI 107.4 ^c N* 67.1 [1.11] Cr 6.3	
A*-P^d		Iso 109.5 [11.76] N* 87.6 [5.43] SmA 79.7 [2.03] Cr 0	
A-Pnd		Iso 182.2 [0.94] BPI 180.7 ^c N* 106.2 [2.44] SmA 72.5 [1.22] Cr 1.5	
A*-Pnd		Iso 108.0 [0.36] BPI 76.6 ^c N* 51.9 [1.63] Cr 31.4	

^a Peak temperatures in the DSC profiles obtained during the first heating and cooling cycles at a rate of 1 °Cmin⁻¹. ^b Iso = isotropic phase; BPI = blue phase I; N* = chiral nematic phase; SmA = smectic A phase; Cr = crystal; ^c The transition to this phase was observed under the polarizing optical microscope and it was too weak to be recognized by the DSC. ^d The analogous covalent diads (see reference 33). The phase transition temperatures and enthalpies of complexes upon heating and those of pure components **A** and **AF*** are shown in Tables S4 and S5, respectively.

A*/P* (1:1 mol.). However, H-bonded dimeric complex **A*/P** (1:1 mol.) with a dipole moment of 6.0 D and a bent angle of 152.9° has a broader BPI temperature range than the analogous covalent diad **A-P*** with a dipole moment of 13.2 D and a bent angle of 141.1°. In general, H-bonded dimeric complexes possess smaller dipole moments (5.8-7.4 D) and larger bent angles (149.9°-162.0°) in contrast to those (11.9-13.2 D and 126.5°-141.1°, respectively) of their analogous covalent diads. However, the large variations of dipole moments in H-bonded dimeric complexes and their analogous covalent diads will not affect the presence of the blue phase. We found that the bent angle plays an important role to manipulate the existence of the blue phase, which is preferred to appear at the bent angle ranging 132.1°-152.9°. Thus, due to lacks of proper bent angles within 132.1°-152.9°, both H-bonded dimeric complex **A/P*** and covalent diad **A*-P** (with bent angles of 162.0° and 126.5°, respectively) did not possess any blue phase.

Optical and XRD investigations

As shown in Fig. 3, a typical schlieren texture⁴⁷ with four brushes at 145.3°C in Fig. 3 (a) and a fingerprint texture at 139.2°C in Fig. 3 (b) were observed in the asymmetric H-bonded dimeric complexes **AF/P** (1:1 mol.) and **A/P*** (1:1 mol.), respectively. Regarding the mesophases of asymmetric H-bonded dimeric complexes **AF*/P** (3:1 mol.) and **AF*/P*** (3:1 mol.), we investigated the phase transition sequence by POM on the cooling process with a cooling rate of 0.5 °Cmin⁻¹. Figs. 4(a)-4(d) show the phase transition sequence of **AF*/P** (3:1 mol.): the isotropic phase (Iso)-blue phase I (PBI) which has platelet textures with different colors and fine stripes-chiral nematic phase (N*)-homeotropic state of the Smectic A phase (the inset is the conoscopic pattern), respectively. Similarly, the phase transition sequence of **AF*/P*** (3:1 mol.) is shown in Fig. 5(a)-5(c): Iso-BPI-N*, respectively.

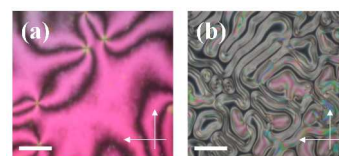


Fig. 3 POM texture shows the phase transition process of asymmetric H-bonded dimeric complexes (a) **AF/P** (1:1 mol.) the nematic phase at 145.3°C and (b) **A/P*** (1:1 mol.) the chiral nematic phase at 139.2°C. On cooling rate 0.5 °Cmin⁻¹.

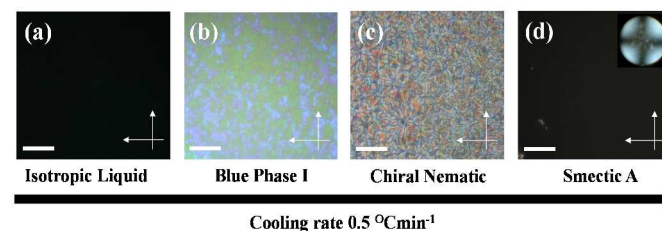


Fig. 4 POM texture shows the phase transition process of the asymmetric H-bonded dimeric complex **AF*/P** (3:1 mol.). On cooling rate 0.5 °Cmin⁻¹. (a) The isotropic liquid at 112.1°C. (b) The blue phase I (platelet textures with different colors and fine stripes) at 102.8°C. (c) The chiral nematic phase at 96.2°C. (d) homeotropic texture of the Smectic A phase (inset picture is conoscopic pattern) at 75.1°C. (Scale bar: 40µm. White arrows are the directions of polarizers and analyzers.)

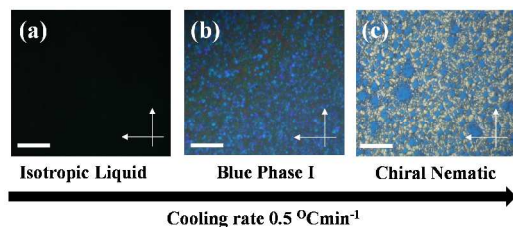


Fig. 5 POM texture shows the phase transition process of the asymmetric H-bonded dimeric complex AF^*/P^* (3:1 mol.). On cooling rate $0.5\text{ }^\circ\text{Cmin}^{-1}$. (a) The isotropic liquid at 115.1°C . (b) The blue phase I (platelet textures with different colors and fine stripes) at 101.2°C . (c) The chiral nematic phase at 75.1°C . (Scale bar: $40\mu\text{m}$. White arrows are the directions of polarizers and analyzers.)

All phase transition sequences were investigated by XRD measurements (see Fig. S1 and Table S1). The sharp reflection peaks of XRD patterns (representing d-spacing layer) were observed in the small angle area of the smectic phase (including SmA), but only broad peaks were revealed in the wide angle area of the N and N^* phases. As shown in Table S1 (see the supporting information), A/P (1:1 mol.), A^*/P (1:1 mol.), AF/P (1:1 mol.) and AF^*/P (1:1 mol.) possessed d-spacing values of 48.1 \AA , 47.5 \AA , 47.8 \AA and 46.7 \AA , respectively. In addition, A/P^* (1:1 mol.), A^*/P^* (1:1 mol.) and AF/P^* (1:1 mol.) also exhibited d-spacing values of 48.5 \AA , 47.7 \AA and 49.1 \AA , respectively. Their d-spacing values (d) were similar to their corresponding molecular lengths (L) by the theoretical simulation (shown below), which suggested the d-spacing values of the SmA phase in these diads are monolayer arrangements (i.e., $d \sim L$). Therefore, the SmA phase was verified not only by the homeotropic texture of POM photo-images but also by the sharp peaks (d-spacing values) of XRD measurements.

Theoretical simulation

To substantiate the structural changes observed in the experiment for the eight asymmetric H-bonded dimeric complexes and to provide a better insight into the effects of the temperature range and stabilization on BPs (see Table 3 and the Supporting Information). We have a detailed quantum chemical calculation for the geometrical parameters of hydrogen bond lengths, molecular lengths, breadth, bent angles, dipole moments and charge density distribution properties. The electronic optimization for all asymmetric H-bonded dimeric complexes D/P and D/P^* ($\text{D} = \text{A}, \text{A}^*, \text{AF}$ and AF^*) in the gas-phase was carried out at the B97D/6-31G(d,p) level. Among all eight complexes, four structures of asymmetric H-bonded dimeric

Table 3 Calculated lengths, breadths, bent angles and dipole moments of the optimized asymmetric H-bonded dimeric complexes at the B3LYP level with the 6-31G(d) basis set

Complex (1:1 mol.)	Length L (\AA)	Breadth W_1 (\AA)	Breadth W_2 (\AA)	Biaxial parameter (W_1/W_2)	H-bond length (\AA)	H-bond bent angle (deg)	Bent angle (deg) ^a	Dipole moment (Debye, D)	HTP (μm^{-1}) ^b
A^*/P	46.7	9.5	4.9	1.94	1.7	178.3	152.9	6.0	2.56
A^*/P^*	46.5	9.3	6.0	1.55	1.7	178.8	150.6	6.6	2.78
AF^*/P	46.7	9.6	4.9	1.96	1.7	178.5	152.5	6.7	2.50
AF^*/P^*	46.4	9.4	6.2	1.52	1.7	178.5	149.9	7.4	2.94

^a Bent angle ($^\circ$) measured as the angle between the first, central and final benzene rings' centers of the bent-core structures. The detailed dipole moments of the lowest energy structures are given (see Tables S2 and S3 of

the Supporting Information). ^b HTP values of H-bonded complexes and analogous covalent diads (see Table S2) were obtained by Cano wedge cells.

complexes are more efficient for the formation of BPs, including A^*/P (1:1 mol.), AF^*/P (1:1 mol.), A^*/P^* (1:1 mol.) and AF^*/P^* (1:1 mol.), bearing the chiral center (on H-donor and/or H-acceptor) and the lateral fluoro substituent. Their main geometrical parameters are summarized in Table 3 and structures are shown in Fig. 6. The geometrical properties of the remaining complexes A/P (1:1 mol.), AF/P (1:1 mol.), A/P^* (1:1 mol.) and AF/P^* (1:1 mol.) are shown in Fig. S2 and Tables S2 and S3 of the Supporting Information. Because the biaxiality, bent angle and dipole moment of the molecule play a very important role in the widening and stabilizing the BP temperature range, these parameters are defined as follows: L (length along the long axis), biaxiality equals W_1/W_2 (W_1 : width along the short axis normal to the benzene plane and W_2 : width along the short axis parallel to the benzene plane) and bent angles are measured as the angles between the centers of the first, central and final benzene rings of the bent-core structures (as shown in Fig. 6). The calculated hydrogen bond lengths and hydrogen bond bent angles in complexes A^*/P (1:1 mol.), AF^*/P (1:1 mol.), A^*/P^* (1:1 mol.) and AF^*/P^* (1:1 mol.) are almost similar and ca. 1.7 \AA and 178° , respectively.

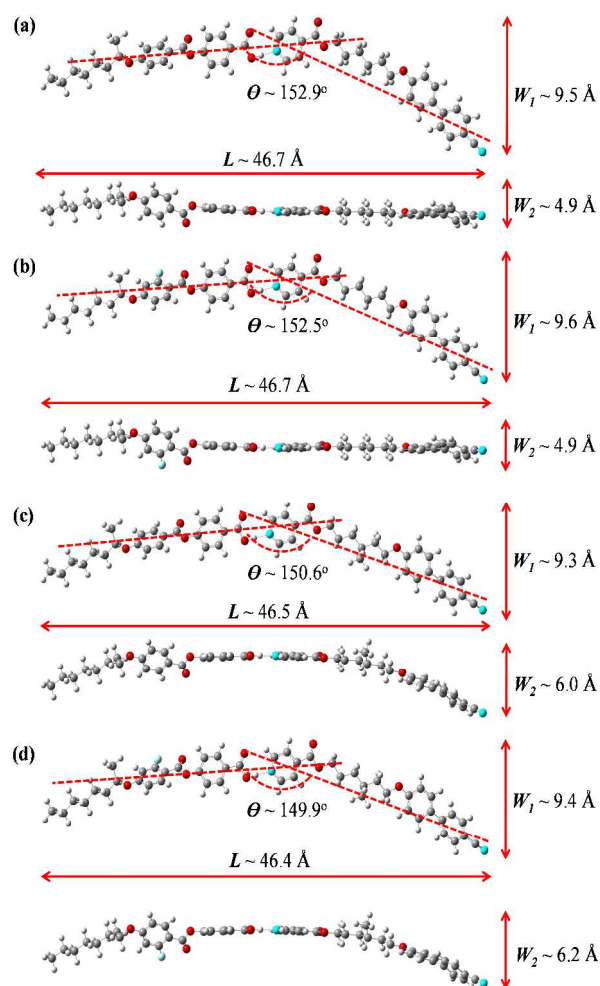


Fig. 6 Optimized geometries of asymmetric H-bonded dimeric complexes (a) A^*/P (1:1 mol.), (b) AF^*/P (1:1 mol.), (c) A^*/P^* (1:1 mol.) and (d) AF^*/P^* (1:1 mol.) are computed with the B97D/6-31G(d,p) method and shows in top and side view.

As shown in Table 3, the HTP values of four H-bonded dimeric complexes with BPs, including A^*/P , AF^*/P , A^*/P^* and AF^*/P^* (1:1 mol.), bearing the chiral center (on H-donor and/or H-acceptor) and the lateral fluoro substituent are listed and compared with their analogous covalent diads (including A^*-P , $A-P^*$ and A^*-P^* in Table S2). All H-bonded dimeric complexes A^*/P ($2.56 \mu\text{m}^{-1}$), A/P^* ($2.44 \mu\text{m}^{-1}$) and A^*/P^* ($2.78 \mu\text{m}^{-1}$) have smaller HTP values than their analogous covalent diads A^*-P ($3.05 \mu\text{m}^{-1}$), $A-P^*$ ($2.97 \mu\text{m}^{-1}$) and A^*-P^* ($3.22 \mu\text{m}^{-1}$), respectively, where the lower HTP values of H-bonded dimeric complexes might be attributed to the higher flexibilities of their H-bonded structures. Moreover, the HTP values of H-bonded dimeric complexes have the trend of $A^*/P^* > A^*/P > A/P^*$ similar to that of covalent diads $A^*-P^* > A^*-P > A-P^*$. Hence, the highest HTP values of A^*/P^* and A^*-P^* (with two chiral centers) along with the lowest HTP values of A/P^* and $A-P^*$ (with a single chiral center on the middle of the flexible spacer) are obtained in both H-bonded complexes and covalent diads, respectively.

(i) Complexes D/P^* and D/P (where $D = A^*$ and AF^*)

The BP temperature range of asymmetric H-bonded dimeric complexes D/P^* ($D = A^*$ and AF^*) (chiral center on H-acceptor) as compared with complexes D/P ($D = A^*$ and AF^*) (non-chiral center on H-acceptor) at molar ratio of H-acceptors (P and P^*) and H-donors (A^* and AF^*) is 1:1. The asymmetric H-bonded dimeric complexes AF^*/P^* (1:1 mol.) $\sim 6.0^\circ\text{C}$ and A^*/P^* (1:1 mol.) $\sim 4.7^\circ\text{C}$ are much wider than AF^*/P (1:1 mol.) $\sim 5.6^\circ\text{C}$ and A^*/P (1:1 mol.) $\sim 2.4^\circ\text{C}$, because complexes D/P^* ($D = A^*$ and AF^*) have one more chiral center on H-acceptor than complexes D/P ($D = A^*$ and AF^*). We further investigate the deviations of biaxiality, dipole moment and bent angle between both complexes D/P^* and D/P ($D = A^*$ and AF^*). The results show that the performance of biaxiality for complexes A^*/P (1:1 mol.) and AF^*/P (1:1 mol.) (biaxiality parameter ~ 1.94 and ~ 1.96 , respectively) is greater than complexes A^*/P^* (1:1 mol.) and AF^*/P^* (1:1 mol.) (biaxiality parameter ~ 1.55 and ~ 1.52 , respectively). The bent angle and dipole moment results of A^*/P^* (1:1 mol.) (bent angle $\sim 150.6^\circ$ and dipole moment ~ 6.6 D) and AF^*/P^* (1:1 mol.) (bent angle $\sim 149.9^\circ$ and dipole moment ~ 7.4 D) indicate a greater bent shape and larger dipole moment value than A^*/P (1:1 mol.) (bent angle $\sim 152.9^\circ$ and dipole moment ~ 6.0 D) and AF^*/P (1:1 mol.) (bent angle $\sim 152.5^\circ$ and dipole moment ~ 6.7 D), respectively. Hence, the chiral center is introduced to H-acceptor to increase the value of dipole moment and bent shape of molecule; thus it is more helpful to stabilize and extend the BP temperature range than biaxiality.

(ii) Complexes AF^*/N and A^*/N (where $N = P$ and P^*)

Next, we investigated the changes of BP temperature range that took place on the lateral fluoro substituent at H-donors of asymmetric H-bonded dimeric complexes AF^*/N ($N = P$ and P^*) compared with those without lateral fluoro substituent at H-donors of complexes A^*/N ($N = P$ and P^*). The experimental results of BP temperature range show that the complexes AF^*/P^* (1:1 mol.) $\sim 6.0^\circ\text{C}$ and

AF^*/P (1:1 mol.) $\sim 5.6^\circ\text{C}$ are much wider than A^*/P^* (1:1 mol.) $\sim 4.7^\circ\text{C}$ and A^*/P (1:1 mol.) $\sim 2.4^\circ\text{C}$ complexes. Our theoretical results show that the molecular bent angles and dipole moment values of lateral fluoro substituent complexes AF^*/P (1:1 mol.) and AF^*/P^* (1:1 mol.) are greater than those without fluorine substitution complexes A^*/P (1:1 mol.) and A^*/P^* (1:1 mol.) (See Table 3). As alluded to above, we concluded that the lateral fluoro substituent at H-donors delivered a high electronegativity and dipole moment, hence the fluorine is more favourable to broaden the BP range. Although the performance of biaxiality for complex AF^*/P^* (1:1 mol.) is only 1.52, complex AF^*/P^* (1:1 mol.) has a large value of dipole moment (~ 7.4 D) and a bent shape of molecular geometry ($\sim 149.9^\circ$). The results show that the ground state dipole moments for all complexes based on the Cartesian coordinate system are found to be oriented in XY-plane and mainly dominant on the X axis, lying on the backbones of the molecule (see Supporting Information Table S3). In this study, the molar ratio H-donors (AF^*) vs. H-acceptors (P^*) was 3:1 (75 mole%) which exhibited the widest temperature range of BP ($\sim 13.2^\circ\text{C}$). In addition to the analysis of the electron density distribution properties, we also generated the electrostatic potential of asymmetric H-bonded dimeric complexes A^*/P (1:1 mol.), AF^*/P (1:1 mol.), A^*/P^* (1:1 mol.) and AF^*/P^* (1:1 mol.) at the B97D/6-31G(d,p) level which is shown in Fig. S4 to get a better understanding of its chemical reactivity (the other asymmetric H-bonded dimeric complexes are also shown in Fig. S3 of the supporting information). The charge distributions in molecules can be displayed by electron-rich (red; δ^-) and electron-poor (blue; δ^+).

Conclusions

In this work, a series of novel asymmetric H-bonded dimeric complexes D/P and D/P^* (where $D = A, A^*, AF$ and AF^*) were synthesized and self-assembled by different molar ratios of H-donors (A, A^*, AF and AF^*) and H-acceptors (P and P^*), where the chiral centers were introduced into the linker of H-acceptors (P and P^*) and/or the flexible terminus of H-donors (A^* and AF^*) to study the H-bonded effects on the presence of BPs. In addition, the influences of the lateral fluoro-substituent of H-donors (AF and AF^*) on the mesophasic behaviours (e.g., BPs) of asymmetric H-bonded dimeric complexes are investigated. Moreover, H-bonded dimeric complex AF^*/P^* (1:1 mol.) with the widest BP range of 6.0°C in this report can be further optimized to exhibit even wider temperature range of BPI ($\sim 13.2^\circ\text{C}$) by a molar ratio of 3:1 due to the excessive acid dimmer AF^* acted as a chiral dopant. Comparing the BPs of H-bonded dimeric complexes A^*/P , A/P^* and A^*/P^* with those of our previously reported analogous covalent diads A^*-P , $A-P^*$ and A^*-P^* , respectively, the bent angle plays an important role to control the blue phase, which is preferred to exist at the bent angle between 132.1° - 152.9° . Therefore, due to unsuitable bent angles, both H-bonded dimeric complex A/P^* and covalent diad A^*-P (with bent angles of 162.0° and 126.5° , respectively) did not possess any blue phase. Finally, the H-bonded effects of chiral centers and lateral fluoro-substituent on supramolecular mesophasic structures via theoretical calculation of biaxiality, bent angle and dipole moment are useful to extend and stabilize the temperature ranges of BPs.

Acknowledgements

The financial supports of this project are provided by the Ministry of Science and Technology (MOST) in Taiwan through MOST 103-2113-M-009-018-MY3 and MOST 103-2221-E-009-215-MY3. The powder XRD measurements were supplied by beam-line BL17A (charged by Dr Jey-Jau Lee) of the National Synchrotron Radiation Research Center (NSRRC) in Taiwan.

Notes and references

1. H. Kikuchi, *Struct Bond*, 2008, **128**, 99–117.
2. L. Rao, Z. Ge, S. Gauza, K. M. Chen and S. T. Wu, *Mol. Cryst. Liq. Cryst.*, 2010, **527**, 30–42.
3. Y. H. Lin, H. S. Chen, H. C. Lin, Y. S. Tsou, H. K. Hsu and W. Y. Li, *Appl. Phys. Lett.*, 2010, **96**, 113505-1–113505-3.
4. Y. H. Lin, H. S. Chen, T. H. Chiang, C. H. Wu, and H. K. Hsu, *Opt. Express*, 2011, **19**, 2556–2561.
5. W. Cao, A. Munoz, P. Palfy-Muhoray and B. Taheri, *Nat. Mater.*, 2002, **1**, 111–113.
6. J. Yan, L. Rao, M. Jiao, H. C. Cheng and S. T. Wu, *J. Mater. Chem.*, 2011, **21**, 7870–7877.
7. S. Yokoyama, S. Mashiko, H. Kikuchi, K. Uchida and T. Nagamura, *Adv. Mater.*, 2006, **18**, 48–51.
8. F. Castles, F. V. Day, S. M. Morris, D. H. Ko, D. J. Gardiner, M. M. Qasim, S. Nosheen, P. J. W. Hands, S. S. Choi, R. H. Friend and H. J. Coles, *Nat. Mater.*, 2012, **11**, 599–603.
9. H.-S. Kitzerow, *Chem. Phys. Chem.*, 2006, **7**, 63–66.
10. A. Yoshizawa, *RSC Adv.*, 2013, **3**, 25475–25497.
11. O. Jin, D. Fu, J. Wei, H. Yang and J. Guo, *RSC Adv.*, 2014, **4**, 28597–28600.
12. H. Stegemeyer, Th. Blumel, K. Hiltrop, H. Onusseit and F. Porsch, *Liq. Cryst.*, 1986, **1**, 3–28.
13. E. Dubois-Violette and B. Pansu, *Mol. Cryst. Liq. Cryst.*, 1988, **165**, 151–182.
14. J. A. N. Zasadzinski, S. Meiboom, M. J. Sammon and D. W. Berreman, *Phys. Rev. Lett.*, 1986, **57**, 364–367.
15. O. Henrich, K. Stratford, M. E. Cates and D. Marenduzzo, *Phys. Rev. Lett.*, 2011, **106**, 107801-1–107801-4.
16. I. Dierking, W. Blenkhorn, E. Credland, W. Drake, R. Kociuruba, B. Kayser and T. Michael, *Soft Matter*, 2012, **8**, 4355–4362.
17. H. Kikuchi, M. Yokota, Y. Hisakado, H. Yang and T. Kajikawa, *Nat. Mater.*, 2002, **1**, 64–68.
18. H. J. Coles and M. N. Pivnenko, *Nature*, 2005, **436**, 997–1000.
19. A. Yoshizawa, Y. Kogawa, K. Kobayashi, Y. Takanishi and J. Yamamoto, *J. Mater. Chem.*, 2009, **19**, 5759–5764.
20. M. Sato and A. Yoshizawa, *Adv. Mater.*, 2007, **19**, 4145–4148.
21. M. Tanaka and A. Yoshizawa, *J. Mater. Chem. C.*, 2013, **1**, 315–320.
22. L. Wang, W. He, X. Xiao, F. Meng, Y. Zhang, P. Yang, L. Wang, J. Xiao, H. Yang and Y. Lu, *Small*, 2012, **8**, 2189–2193.
23. S. Taushanoff, K. Van Le, J. Williams, R. J. Twieg, B. K. Sadashiva, H. Takezoe and A. Jákli, *J. Mater. Chem.*, 2010, **20**, 5893–5898.
24. I. H. Chiang, C. J. Long, H. C. Lin, W. T. Chuang, J. J. Lee and H. C. Lin, *Appl. Mater. Interfaces*, 2014, **6**, 228–235.
25. H. Chen, Y. Liu, T. Gong, L. Wang, K. Zhao and S. Zhou, *RSC Adv.*, 2013, **3**, 7048–7056.
26. Y. Arakawa, S. Kang, J. Watanabe and G. I. Konishi, *RSC Adv.*, 2015, **5**, 8056–8062.
27. A. Paikar, A. Pramanik and D. Haldar, *RSC Adv.*, 2015, **5**, 31845–31851.
28. W. L. He, M. J. Wei, H. Yang, Z. Yang, H. Cao and D. Wang, *Phys. Chem. Chem. Phys.*, 2014, **16**, 5622–5626.
29. Y. Shi, X. Wang, J. Wei, H. Yang and J. Guo, *Soft Matter*, 2013, **9**, 10186–10195.
30. W. He, G. Pan, Z. Yang, D. Zhao, G. Niu, W. Huang, X. Yuan, J. Guo, H. Cao, and H. Yang, *Adv. Mater.*, 2009, **21**, 2050–2053.
31. J. Guo, Y. Shi, X. Han, O. Jin, J. Wei and H. Yang, *J. Mater. Chem. C*, 2013, **1**, 947–957.
32. Y. Li, Y. Cong, H. Chu and B. Zhang, *J. Mater. Chem. C*, 2014, **2**, 1783–1790.
33. C. L. Wei, T. C. Chen, P. Raghunath, M. C. Lin and H. C. Lin, *RSC Adv.*, 2015, **5**, 4615–4622.
34. M. J. Frisch, G. W. Trucks, H. B. Schlegel *et al.*, Gaussian 09, Revision A.1. Gaussian, Inc., Wallingford CT, 2009.
35. S. Grimme, *J. Comp. Chem.* 2006, **27**, 1787–1799.
36. B. H. Besler, K. M. Merz Jr. and P. A. Kollman, *J. Comp. Chem.*, 1990, **11**, 431–439.
37. C. Osuji, C. Y. Chao, I. Bitá, C. K. Ober and E. L. Thomas, *Adv. Funct. Mater.*, 2002, **12**, 753–758.
38. Q. Wei, L. Shi, H. Cao and H. Yang, *Liq. Cryst.*, 2007, **34**, 855–860.
39. C. W. Wu and H. C. Lin, *Macromolecules*, 2006, **39**, 7985–7997.
40. L. Y. Wang, S. Y. Tsa and H. C. Lin, *Macromolecules*, 2010, **43**, 1277–1288.
41. P. J. Yang, L. Y. Wang, C. Y. Tang and H. C. Lin, *J. Polym. Sci., Part A: Polym. Chem.*, 2010, **48**, 764–774.
42. T. Kato and J. M. J. Frechet, *J. Am. Chem. Soc.*, 1989, **111**, 8533–8534.
43. Y. Q. Tian, Y. J. Zhang, Y. Y. Zhao and X. Y. Tang, *Chem. J. Chinese U.*, 1997, **18**, 1715–1718.
44. T. Kato, J. M. J. Frechet, P. G. Wilson, T. Saito, T. Uryu, A. Fujishima, C. Jin and F. Kaneuchi, *Chem. Mater.*, 1993, **5**, 1094–1100.
45. M. Hird, *Chem. Soc. Rev.*, 2007, **36**, 2070–2095.
46. M. Lee, S. T. Hur, H. Higuchi, K. Song, S. W. Choi and H. Kikuchi, *J. Mater. Chem.*, 2010, **20**, 5813–5816.
47. I. Dierking and P. Archer, *RSC Adv.*, 2013, **3**, 26433–26437.

Table of contents (TOC)/graphical abstract

The number/position of chiral centers and the molar ratios of H-donors/H-acceptors affect the blue phase ranges of asymmetric H-bonded complexes.

